

## Different regimes of Förster-type energy transfer between an epitaxial quantum well and a proximal monolayer of semiconductor nanocrystals

Š. Kos,<sup>1,\*</sup> M. Achermann,<sup>2</sup> V. I. Klimov,<sup>2</sup> and D. L. Smith<sup>1</sup>

<sup>1</sup>*Theoretical Division, Los Alamos National Laboratory, Los Alamos, New Mexico 87545, USA*

<sup>2</sup>*Chemistry Division, Los Alamos National Laboratory, Los Alamos, New Mexico 87545, USA*

(Received 24 May 2004; revised manuscript received 10 December 2004; published 20 May 2005)

We calculate the rate of nonradiative, Förster-type energy transfer (ET) from an excited epitaxial quantum well (QW) to a proximal monolayer of semiconductor nanocrystal quantum dots (QDs). Different electron-hole configurations in the QW are considered as a function of temperature and excited electron-hole density. A comparison of the theoretically determined ET rate and QW radiative recombination rate shows that, depending on the specific conditions, the ET rate is comparable to or even greater than the radiative recombination rate. Such efficient Förster ET is promising for the implementation of ET-pumped, nanocrystal QD-based light emitting devices.

DOI: 10.1103/PhysRevB.71.205309

PACS number(s): 73.21.La, 78.67.Hc

### I. INTRODUCTION

Modern colloidal chemistry allows the fabrication of semiconductor nanocrystal quantum dots (QDs) with nearly atomic precision in a wide range of sizes and shapes.<sup>1–6</sup> Nanocrystal QDs exhibit high photoluminescence (PL) quantum yields<sup>3–5</sup> and size-controlled emission spectra. Nanocrystals can also be easily manipulated into various two-dimensional (2D) and three-dimensional (3D) assemblies.<sup>7–9</sup> All of these properties make nanocrystal QDs attractive building blocks for various optical devices including color-selectable light emitters. A major problem associated with the realization of nanocrystal QD-based light emitters is that the electrical injection of carriers into nanocrystals is complicated by the presence of an insulating passivation layer. All previous attempts to electrically contact nanocrystals have utilized hybrid inorganic/organic composites comprising conducting polymers.<sup>10–13</sup> However, the performance of these devices is severely limited by low carrier mobilities in both nanocrystal and polymer components and poor polymer stability with respect to photooxidation.

Recently, we have presented an alternative, “noncontact” approach to injecting carriers into nanocrystal QDs via nonradiative energy transfer (ET) from a proximal epitaxial quantum well (QW).<sup>14</sup> The experiments revealed efficient energy outflow from the QW, which was accompanied by a complementary energy inflow into a dense monolayer of nanocrystals assembled on top of the QW. The measured ET rates were very fast allowing for the efficient pumping of nanocrystal QDs.

In this paper we develop the theoretical framework to model Förster-type ET from an epitaxial QW to a monolayer of nanocrystal QDs. Our approach is conceptually similar to the theory pioneered by Agranovich and co-workers<sup>15,16</sup> who studied ET from a QW to an adjacent, infinitely thick layer of organic molecules. In addition to considering a different type of acceptors (semiconductor nanocrystals versus organic molecules), and a different “geometry” of the ET system (ET to a single proximal monolayer versus ET to an infinitely thick layer), in the present work we calculate both ET and

radiative decay rates, which allows us to analyze the ET efficiency as a function of temperature and excitation density. We consider the situations for which the electronic excitations in the QW are present either in the form of free electrons and holes or Coulombically bound electron-hole pairs (excitons). We also account for the effects of exciton localization at defect states. Furthermore, we consider two types of resonant QD acceptor states that can be treated either as a dense quasicontinuum (applicable to high-energy QD states located well above the band edge) or the narrow, atomiclike resonances (applicable to near-band-edge QD states). Finally, we apply the developed theory to model our experiments on energy transfer between the InGaN QW and a proximal monolayer of CdSe nanocrystal QDs. We find a remarkable agreement between our experimental observations and the results of the calculations performed for the case of free electrons and holes in the QW. Independent studies of pump-intensity-dependent QW PL confirm that under our experimental conditions the QW excitations can indeed be well described in terms of unbound electrons and holes.

The paper is organized as follows. We introduce the general formalism in Sec. II. Then, in Secs. III and IV, we study coupling of QW excitations to high-energy states of the QDs that form a dense, quasicontinuous spectrum. In Sec. III, we investigate the excitation density and temperature regime, in which the excited electron-hole pairs in the QW are bound into noninteracting excitons described by classical statistics. At high temperatures within this regime, the excitons are mobile in the QW and the Förster rate dominates the radiative decay rate. At lower temperatures, the localization of excitons at defects decreases the efficiency of Förster ET. In Sec. IV, we study the density and temperature regime, in which the carriers form a 2D plasma in the QW. As the carrier density increases for a given temperature, the plasma experiences a transition from the nondegenerate to the degenerate regime. In this case, we find that the Förster rate is always greater than the radiative rate and both rates reach maximum around the degeneracy temperature for the holes.

In Sec. V, we examine the case in which QW excitations couple to discrete, low-lying QD states with linewidths that

are smaller than the characteristic energy of the motion of charge carriers in the QW. We find that the ET rate decays exponentially with increasing QW-QD distance in contrast to the power law found for the situation in which the ET occurs into the quasicontinuum of high-energy QD states.

Finally, in Sec. VI, we describe experimental results obtained for the ET structure composed of an InGaN QW and CdSe QDs. The analysis of these results indicates that the nondegenerate free carrier case best describes the structure studied experimentally. We compare the ET rates, radiative decay rates, and ET efficiencies obtained from the theory with those measured experimentally and find good agreement.

A summary of our results is presented in Sec. VII.

## II. GENERAL FRAMEWORK

The geometry of the studied structure is shown in Fig. 1. We consider an epitaxial semiconductor heterostructure, where a QW has been grown between a thick bottom and a thin top barrier layer. On top of the QW structure a monolayer of nanocrystal QDs has been assembled. The derived formulas are not material specific; the numerical values of the ET rates are computed in the subsequent sections for a combination of an InGaN QW and CdSe nanocrystal QDs. The distance  $R$  between the centers of the QD and the QW is determined by the QW and the top barrier widths, the length of the ligand molecules, which surround the QD, and the QD size. We shall simplify the calculations by assuming that the size of the QDs and the width of the QW are small compared

to  $R$ . In the experiments described in Ref. 14, these quantities are of the same order of magnitude as  $R$ . However, taking into account the actual dimensions of the QDs and the QW changes the results by a few percent only (as verified by exact calculations assuming a non-zero width of the QW).

The Förster process transfers an electron-hole excitation from the QW to the QD via the electrostatic interaction

$$H_I^F = \frac{e^2}{\epsilon} \int d^3r_D d^3r_W \sum_{\alpha,\beta} \frac{\psi_\alpha^\dagger(\mathbf{r}_D) \psi_\alpha(\mathbf{r}_D) \psi_\beta^\dagger(\mathbf{r}_W) \psi_\beta(\mathbf{r}_W)}{|\mathbf{r}_D - \mathbf{r}_W|}, \quad (1)$$

where  $\epsilon$  is the average of the high frequency dielectric constants of the QW and air. The initial and final states participating in ET are

$$|i\rangle = |ex_W\rangle |GS_D\rangle \quad (2)$$

and

$$|f\rangle = |GS_W\rangle |ex_D\rangle, \quad (3)$$

where  $|GS\rangle$  and  $|ex\rangle$  are the ground state and the excited state, respectively (subscripts “W” and “D” denote QW and QD, respectively). The matrix elements of the density operators in the numerator of Eq. (1) are zero for our initial and final states, therefore, we use the dipolar expansion of the matrix element. The conduction and valence bands have  $s$  and  $p$  symmetry, respectively, so the dipolar matrix elements are nonzero. Thus, we can use the dipolar approximation for the transition matrix element for a single dot

$$\langle f | H_I^F | i \rangle = \frac{e^2}{\epsilon} \int d^2r_W \frac{\mathbf{d}_D^*(\mathbf{r}_D) \cdot \mathbf{d}_W(\mathbf{r}_W) - 3 \left[ \mathbf{d}_D^*(\mathbf{r}_D) \cdot \frac{\mathbf{r}_D - \mathbf{r}_W}{|\mathbf{r}_D - \mathbf{r}_W|} \right] \left[ \mathbf{d}_W(\mathbf{r}_W) \cdot \frac{\mathbf{r}_D - \mathbf{r}_W}{|\mathbf{r}_D - \mathbf{r}_W|} \right]}{|\mathbf{r}_D - \mathbf{r}_W|^3}, \quad (4)$$

with

$$\mathbf{d}(\mathbf{r}) = \Psi(\mathbf{r}, \mathbf{r}) \langle u_v | \mathbf{r} | u_c \rangle, \quad (5)$$

where  $u_c$  and  $u_v$  are the periodic functions that enter the Bloch wave functions for the conduction and valence bands, respectively, and the envelope wave function  $\Psi$  is assumed to vary on a much larger length scale than the lattice constant. To calculate the transition rate from the Fermi Golden Rule, we square the modulus of this matrix element, multiply by the energy-conserving delta function, sum over the final and initial states (weighted with a thermal distribution function), and finally multiply by the number of the dots.

We calculate the radiative transition rate in a QW by using the Fermi Golden Rule with the interaction Hamiltonian

$$H_I^r = -\frac{1}{c} \int d^3r \mathbf{j}(\mathbf{r}) \cdot \mathbf{A}(\mathbf{r}). \quad (6)$$

The transition matrix element now is

$$\langle \mathbf{k}, \lambda | H_I^r | ex_W \rangle \equiv -\frac{1}{c} \int d^3r \langle GS_W | \mathbf{j}(\mathbf{r}) | ex_W \rangle \cdot \langle \mathbf{k}, \lambda | \mathbf{A}(\mathbf{r}) | 0 \rangle, \quad (7)$$

where  $|\mathbf{k}, \lambda\rangle$  is a one-photon state with wave vector  $\mathbf{k}$  and polarization  $\lambda$ , and  $|0\rangle$  is the photon vacuum. Here, we consider only spontaneous emission; stimulated emission may be important for free carriers below the degeneracy temperature discussed in Sec. IV. Using the canonical commutation relations between position and momentum operators, we obtain

$$\langle GS_W | \mathbf{j}(\mathbf{r}) | ex_W \rangle = -iE_G e \mathbf{d}_W(\mathbf{r}), \quad (8)$$

where we have approximated the exciton energy by the band gap energy  $E_G$ . Again, to determine the radiative transition rate, we need to multiply the square of the modulus of this

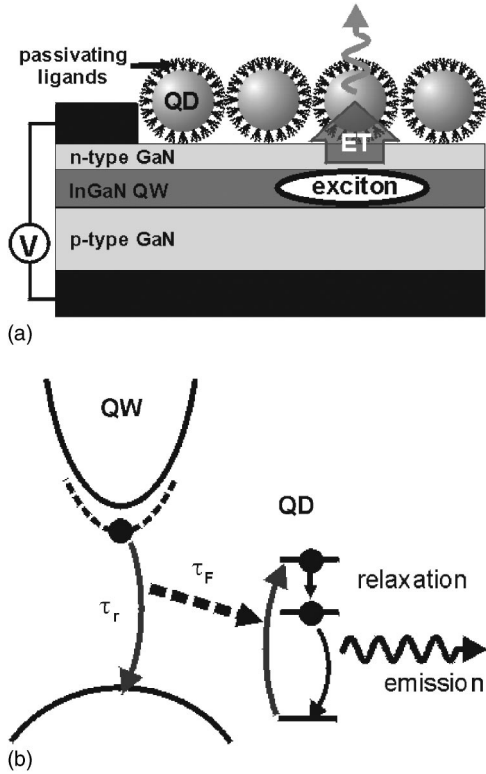


FIG. 1. (a) An example of a hybrid QW/QD structure that can be used for “noncontact” pumping of nanocrystals via nonradiative ET. The structure consists of an InGaN QW sandwiched between GaN barriers. A monolayer of CdSe/ZnS core/shell nanocrystals capped with organic molecules is assembled on the surface of the thin top barrier. The structure is driven electrically using metal contacts attached to the barrier layers. (b) Carrier relaxation and ET processes in the hybrid QW/QD structure. The QW-to-QD ET competes with recombination processes in the QW. High-energy excitations created in the nanocrystals through ET rapidly relax to the nanocrystal band edge, which prevents backtransfer. The relaxed excitations recombine, producing emission with the color determined by the QD size.

transition matrix element by the energy-conserving delta function and sum over all the one-photon states.

### III. EXCITONS IN THE QW

The conduction band is twofold degenerate as a result of the two spin projections; the orbital part of both bands is the same, and has  $s$  symmetry. The valence band is fourfold degenerate in the center of the Brillouin zone, but the spatial confinement in the direction perpendicular to the QW splits the degeneracy. We will only take into account the low-energy, heavy-hole band.

First we consider the case of a free exciton. For the envelope function, we make a separation of variables into the center-of-mass motion described by a plane wave and the relative motion assuming the exciton in a hydrogen  $1s$  state with Bohr radius  $a_B$ . This results in a dipolar matrix element

$$\mathbf{d}_W(\mathbf{r}) = \Psi(\mathbf{r}, \mathbf{r}) \langle u_v | \mathbf{r} | u_c \rangle = \frac{e^{i\mathbf{K} \cdot \mathbf{r}}}{\sqrt{\frac{\pi}{2} A a_B^2}} \frac{d_W}{\sqrt{2}} (\hat{x} \pm i\hat{y}), \quad (9)$$

in which  $A$  is the QW area,  $d_W$  is the QW dipole moment, and  $\mathbf{K}$  is the center-of-mass momentum.

In this case, the matrix element of the Förster transition is

$$\langle f | H_I^F | i \rangle = -\frac{e^2}{\epsilon} \sqrt{\frac{2}{\pi A a_B^2}} (\mathbf{d}_D^* \cdot \nabla) d_W (\partial_x \pm i\partial_y) \phi_{\mathbf{K}}(\mathbf{R}), \quad (10)$$

with

$$\phi_{\mathbf{K}}(\mathbf{R}) \equiv \int d^2 r \frac{e^{i\mathbf{K} \cdot \mathbf{r}}}{|\mathbf{r} - \mathbf{R}|} = 2\pi \frac{e^{i\mathbf{K} \cdot \rho - Kz}}{K}, \quad (11)$$

where  $\rho$  and  $z$  are the in-plane and out-of-plane components of the vector  $\mathbf{R}$ , respectively. The dipolar matrix element of the dot,  $\mathbf{d}_D$ , has a particular value and a random orientation. Squaring the absolute value of the Förster matrix element, averaging over the random direction of  $\mathbf{d}_D$ , summing over the high-energy QD excitons with a smoothly varying density of states  $N_D(E)$ , and summing over the QDs, we obtain the Förster transfer rate (the inverse of the ET time,  $\tau_F$ ),

$$\frac{1}{\tau_F(K)} = \frac{8\pi}{3} \left( \frac{e^2}{\epsilon} \right)^2 |d_D|^2 |d_W|^2 N_D(E_G) \frac{n_D}{a_B^2} K^2 e^{-2KR}, \quad (12)$$

where  $n_D$  is the areal density of the QDs and  $R$  is the QW-QD separation in the  $z$  direction.

To model excitons in a real QW, we have to consider width fluctuations, alloy disorder or impurities that can localize the exciton. If the length scale of such a trap is much larger than  $a_B$ , the relative motion of the exciton will remain unchanged, but the center-of-mass wave function will now be localized instead of being a plane wave. We assume that all the traps in the QW localize the excitons into states with a characteristic binding energy  $E_T$  and localization length  $\xi$ . An analytical evaluation of the matrix elements is possible only for special exciton envelope functions, such as a modified Lorentzian

$$\Psi_{\xi}(r) = \sqrt{\frac{2}{\pi}} \frac{\xi^{-1}}{\left[ 1 + \left( \frac{r}{\xi} \right)^2 \right]^{3/2}}, \quad (13)$$

leading to an ET rate of the bound excitons of

$$\frac{1}{\tau_{F,loc}} = 4\pi \left( \frac{e^2}{\epsilon} \right)^2 |d_D|^2 |d_W|^2 N_D(E_G) n_D \left( \frac{\xi}{a_B} \right)^2 \frac{1}{(\xi + R)^4}. \quad (14)$$

For a different center-of-mass wave function, the functional dependence will be somewhat different, but the asymptotic behavior in the two limits  $\xi \gg R$  and  $\xi \ll R$  will be the same, hence, this is a suitable interpolation between the two limits.

We obtain the total Förster transfer rate by averaging (12) and (14) using the Boltzmann distribution

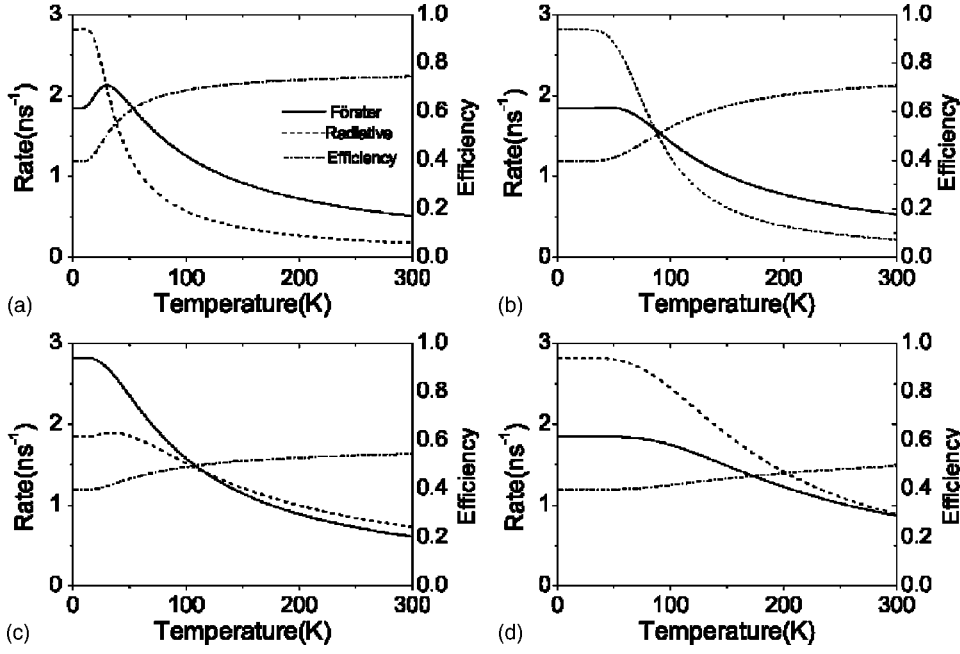


FIG. 2. The Förster (solid line) and radiative (dashed line) transition rates calculated for QW excitons for  $\xi=30$  Å and (a)  $n_T=10^{11}$  cm $^{-2}$  and  $E_T=-0.005$  eV, (b)  $n_T=10^{11}$  cm $^{-2}$  and  $E_T=-0.02$  eV, (c)  $n_T=10^{12}$  cm $^{-2}$  and  $E_T=-0.005$  eV, (d)  $n_T=10^{12}$  cm $^{-2}$  and  $E_T=-0.02$  eV. The dashed-dotted line is the efficiency of the Förster transfer.

$$\frac{1}{\tau_F} = \frac{n_T e^{-\frac{E_T}{T}} \frac{1}{\tau_{F,loc}} + \int \frac{d^2 K}{(2\pi)^2} e^{-\frac{K^2}{2MT}} \frac{1}{\tau_F(K)}}{n_T e^{-\frac{E_T}{T}} + \int \frac{d^2 K}{(2\pi)^2} e^{-\frac{K^2}{2MT}}}$$

$$= 4\pi \left( \frac{e^2}{\epsilon} \right)^2 |d_D|^2 |d_W|^2 N_D(E_G) \frac{n_D}{a_B^2}$$

$$\times \frac{n_T e^{-\frac{E_T}{T}} \frac{\xi^2}{(\xi+R)^4} + \frac{MT}{2\pi} \frac{4}{3R^2} f(2MTR^2)}{n_T e^{-\frac{E_T}{T}} + \frac{MT}{2\pi}}, \quad (15)$$

where  $n_T$  is the areal density of the traps,  $M \equiv m_e + m_h$  is the mass of the exciton, and

$$f(x) \equiv \frac{1}{x} \int_0^\infty d\kappa \kappa^3 e^{-2\kappa - \frac{\kappa^2}{x}}$$

$$= \frac{x}{4} [2(1+x) - e^x \sqrt{\pi x} (3+2x) \text{erfc}(\sqrt{x})]. \quad (16)$$

The performance of a device that relies on ET-pumping of colloidal QDs from a QW is determined by the ET efficiency ( $\eta$ ), which is a function of both the ET rate and the total rate of all recombination processes in the QW ( $\tau_r^{-1}$ ):  $\eta = \tau_F^{-1} / (\tau_F^{-1} + \tau_r^{-1})$ . An ultimate limit on the lifetime of QW excitations is imposed by the radiative decay, which determines an upper limit of the ET efficiency. We calculate the radiative recombination rate from (7). The matrix element of the one-photon transition is

$$\langle \mathbf{k}, \lambda | \mathbf{A}(\mathbf{r}) | 0 \rangle = \sqrt{\frac{2\pi c}{k}} \mathbf{e}_\lambda^*(\mathbf{k}) e^{-i\mathbf{k} \cdot \mathbf{r}}. \quad (17)$$

The integral in (7) will set the in-plane component of  $\mathbf{k}$  equal to  $\mathbf{K}$  and give the radiative rate of a free exciton<sup>17</sup>

$$\frac{1}{\tau_r(K)} = \frac{1}{\pi} (ed_W)^2 \left( \frac{E_G}{c} \right)^2 \frac{1}{a_B^2} \frac{1}{\sqrt{\left( \frac{E_G}{c} \right)^2 - K^2}}$$

$$\times \left( 2 - \frac{c^2 K^2}{E_G^2} \right) \theta(E_G - cK). \quad (18)$$

For a localized exciton, we find

$$\frac{1}{\tau_{r,loc}} = \frac{32}{3\pi} (ed_W)^2 \left( \frac{E_G}{c} \right)^3 \frac{\xi^2}{a_B^2}, \quad (19)$$

resulting in the total recombination rate (obtained by averaging with respect to the Boltzmann distribution)

$$\frac{1}{\tau_r} = \frac{4}{3\pi} (ed_W)^2 \left( \frac{E_G}{c} \right)^3 \frac{1}{a_B^2} \frac{1}{\frac{2\pi}{2\pi} + n_T e^{-\frac{E_T}{T}} 8\xi^2}.$$

$$\frac{1}{\tau_r} = \frac{4}{3\pi} (ed_W)^2 \left( \frac{E_G}{c} \right)^3 \frac{1}{a_B^2} \frac{1}{\frac{MT}{2\pi} + n_T e^{-\frac{E_T}{T}}}. \quad (20)$$

In Fig. 2, we plot the Förster (15) and the radiative (20) transition rates, along with the efficiency of the Förster transfer as a function of temperature. We use the following physical parameters from the experiment in Ref. 14, where a monolayer of CdSe nanocrystal QDs with a 19 Å radius has been deposited on an InGaN QW with a 30 Å width:  $d_D=5.2$  Å,<sup>9</sup>  $d_W=2.9$  Å,<sup>18</sup>  $N_D(E_G)=17.3$  eV $^{-1}$  (determined from the QD absorption spectra),  $E_G=3.1$  eV,  $n_D=2 \times 10^{12}$  cm $^{-2}$ ,  $a_B=27.8$  Å,  $\epsilon=3.6$  [the average of the high frequency dielectric constant of GaN ( $\epsilon_{w,\infty}=6.2$ ) and air ( $\epsilon_{air}=1$ )],  $M=m_e+m_h=0.2m_0+0.8m_0$ ,  $R=81$  Å. In addition, we assume  $\xi=30$  Å (the lower bound for  $\xi$  is  $a_B$ ),  $n_T=10^{11}$  cm $^{-2}$ , and  $E_T=-0.005$  eV in (a) and  $E_T=-0.02$  eV in (b). For the static dielectric constant of GaN  $\epsilon_{w,0}=8.9$ , we obtain the exciton binding energy of 0.0528 eV, which cor-

responds to 675 K. We plot the radiative and ET rates and the ET efficiency up to room temperature, which is roughly half of the latter value.

At high temperatures  $T \gg 1/2MR^2 \approx 5$  K, both  $1/\tau_F$  and  $1/\tau_r$  behave as  $1/T$  with a bigger prefactor for  $1/\tau_F$ . As the temperature decreases, both rates increase, but the increase of  $1/\tau_F$  becomes slower than  $1/T$ , and eventually the two rates cross and  $1/\tau_F$  becomes smaller than  $1/\tau_r$ . The ET efficiency, therefore, increases as the temperature increases up to the crossing point and levels off at temperatures above this point; the individual rates, however, decrease as the temperature is increased further. Thus, the optimum temperature for the ET is around the crossing point between  $1/\tau_F$  and  $1/\tau_r$ , which occurs at temperature on the order of  $1/2MR^2$  if the effect of the exciton localization is negligible. The crossing point shifts to higher temperatures and the ET efficiency is decreased in the case of stronger exciton localization. Localized excitons dominate the rates in the limit  $T \rightarrow 0$ , thus making the rates at the crossing point smaller. Indeed,  $\tau_{r,loc}^{-1}$  grows relative to  $\tau_{F,loc}^{-1}$  with increasing localization length  $\xi$ , and the importance of the localized term grows both with  $n_T$  [compare Figs. 2(a) and 2(b) with Figs. 2(c) and 2(d), respectively] and with  $|E_T|$  [compare Figs. 2(a) and 2(c) with Figs. 2(b) and 2(d), respectively]. We note that the order of magnitude of the transition rates does not change as we vary the localization parameters (compare different panels in Fig. 2).

#### IV. FREE CARRIERS IN THE QW

When the density of electrons or holes  $n_{eh}$ <sup>19</sup> exceeds  $1/a_B^2$  (so that the kinetic energy dominates the Coulomb interaction), or the temperature is higher than the exciton binding energy, then the charge carriers do not form excitons but rather stay unbound. We assume that the energies of the electrons and holes are much larger than  $E_T$ , so that we can treat the charge carriers as free particles described by plane waves

$$\Psi(\mathbf{r}, \mathbf{r}) = \frac{e^{i\mathbf{K}\cdot\mathbf{r}}}{A}. \quad (21)$$

The use of these wave functions modifies the normalization in (12). In the classical (nondegenerate) case, that is  $n_{eh} < 2m_e T/2\pi, 2m_h T/2\pi$ , we can express the ET rate (after averaging over the thermal distribution of free carriers) as

$$\frac{1}{\tau_{F,class}} = \frac{8\pi^2}{3} \left( \frac{e^2}{\epsilon} \right)^2 |d_D|^2 |d_W|^2 N_D(E_G) n_D n_{eh} \frac{1}{R^2} f(2MTR^2). \quad (22)$$

The latter expression indicates that the ET rate in the free-carrier case is proportional to  $n_{eh}$ .

For  $n_{eh} > 2m_e T/2\pi, 2m_h T/2\pi$ , both the electrons and the holes form degenerate Fermi gases and the total Förster rate will be

$$\frac{1}{\tau_{F,deg}} = \sum_{\mathbf{k}_e, \mathbf{k}_h}^{\sqrt{2\pi n_{eh}}} \frac{1}{\tau_F(K)}. \quad (23)$$

We convert the sum over momentum into an integral that can be calculated explicitly, holding  $\mathbf{k}_e + \mathbf{k}_h = \mathbf{K}$ . The Förster rate

per electron-hole ( $e-h$ ) pair in the degenerate regime is

$$\frac{1}{\tau_{F,deg}} = \frac{2}{3} \left( \frac{e^2}{\epsilon} \right)^2 |d_D|^2 |d_W|^2 N_D(E_D) n_D \frac{1}{R^4} g(2\sqrt{2\pi n_{wh} R^2}), \quad (24)$$

where

$$g(x) \equiv x^4 \int_0^1 d\kappa \left( \frac{\pi}{2} - \arcsin \kappa - \kappa \sqrt{1 - \kappa^2} \right) \kappa^3 e^{-2\kappa x}. \quad (25)$$

The corresponding recombination rates will be obtained from the decay rate calculated for a single  $e-h$  pair with the center-of-mass momentum  $\mathbf{K}$ , which is the same as (18) except that  $a_B^2$  in the denominator is replaced with the total QW area  $A$ .

For the classical case ( $n_{eh} < 2m_e T/2\pi, 2m_h T/2\pi$ ), we obtain

$$\frac{1}{\tau_{r,class}} = \frac{2}{3} (ed_w)^2 \left( \frac{E_G}{c} \right)^3 \frac{n_{eh}}{MT}, \quad (26)$$

whereas for the degenerate case,  $n_{eh} > 2m_e T/2\pi, 2m_h T/2\pi$ , the radiative recombination rate is

$$\frac{1}{\tau_{r,deg}} \approx \sum_{\mathbf{k}_e, \mathbf{k}_h}^{\sqrt{2\pi n_{eh}}} \frac{1}{\tau_{r,free}(K)} = \frac{1}{6\pi} (ed_w)^2 \left( \frac{E_G}{c} \right)^3. \quad (27)$$

Finally, if  $m_h \gg m_e$ , we have an intermediate regime

$$2m_e T/2\pi < n_{eh} < 2m_h T/2\pi, \quad (28)$$

that is, the electrons are degenerate and the holes are classical. We can obtain the Förster and radiative rates from formulas (22) and (26), respectively, if we replace  $M$  with

$$m_e \frac{E_{Fe}}{T} + m_h, \quad (29)$$

where  $E_{Fe} = 2\pi n_{eh}/2m_e$ . Since

$$m_e \frac{E_{Fe}}{T} = m_h \frac{2\pi n_{eh}}{2m_h T} < m_h \quad (30)$$

in the intermediate regime, the Förster and radiative rates behave as in the classical regime with the total mass replaced by the mass of the hole.

In Fig. 3, we show the Förster and the radiative transition rates, in the classical/intermediate regime as obtained from formulas (22) and (26), respectively, for  $n_{eh} = 10^{12} \text{ cm}^{-2}$  as a function of temperature (a) and for  $T = 300$  K as a function of  $n_{eh}$  (b). The dashed-dotted line is the efficiency of the Förster transfer. The straight-line segments indicate the asymptotic degenerate values given by formulas (24) and (27) in the limit  $T \rightarrow 0$  (a) ( $0.0749 \text{ ns}^{-1}$  for the Förster rate and  $0.0379 \text{ ns}^{-1}$  for the radiative rate with efficiency 0.66), and in the limit  $n_{eh} \rightarrow \infty$  (b) ( $0.175 \text{ ns}^{-1}$  for the Förster rate and  $0.0379 \text{ ns}^{-1}$  for the radiative rate with efficiency 0.82). Independent of temperature and carrier density, the energy transfer rate is always higher than the radiative transition rate in the QW. In the classical regime both rates scale approxi-

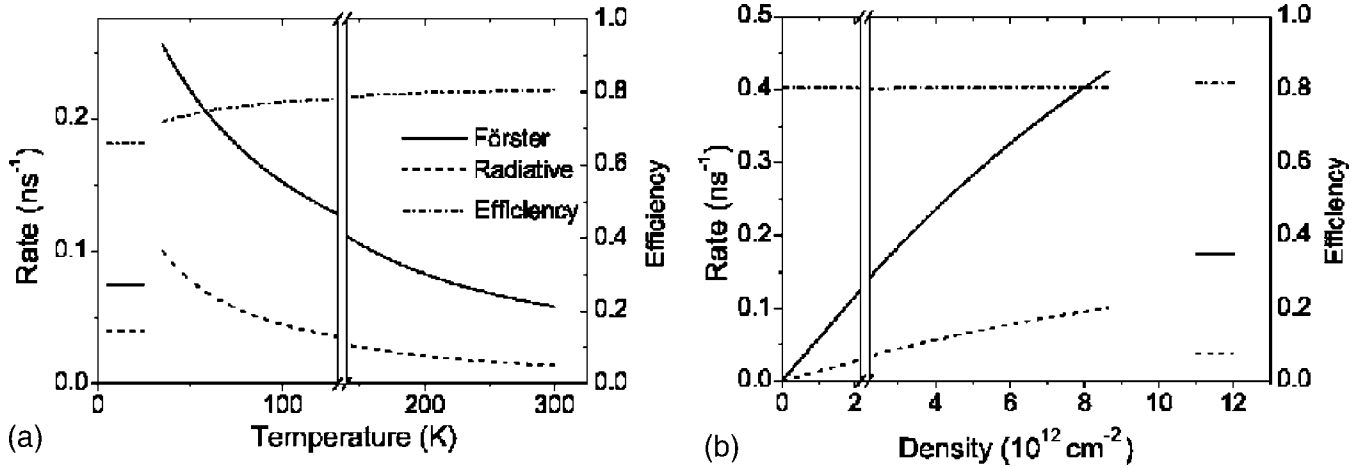


FIG. 3. The Förster (solid line) and radiative (dashed line) transition rates for QW classical free carriers, along with the ET efficiency (dashed-dotted line). (a) The calculations are shown for  $n_{eh}=10^{12}$  cm $^{-2}$  as a function of  $T$  above the degeneracy temperature 34.7 K. (b) The calculations are shown for  $T=300$  K as a function of  $n_{eh}$  below the degeneracy density  $8.6 \times 10^{12}$  cm $^{-2}$ . The straight-line segments indicate the asymptotic degenerate values in the limit  $T \rightarrow 0$  for the Förster (0.0749 ns $^{-1}$ ) and radiative (0.0379 ns $^{-1}$ ) rates with efficiency 0.66 (a), and in the limit  $n_{eh} \rightarrow \infty$  for the Förster (0.175 ns $^{-1}$ ) and radiative (0.0379 ns $^{-1}$ ) rates with efficiency 0.82 (b).

mately as  $1/T$  and are linear in  $n_{eh}$ , whereas in the degenerate case  $1/\tau_F$  and  $1/\tau_r$  are only weakly dependent on temperature and carrier density. The crossover between the degenerate and the intermediate regime is very pronounced and occurs at 34.7 K (a) and  $8.6 \times 10^{12}$  cm $^{-2}$  (b). The crossover between the intermediate and classical regime is at temperature  $2\pi n_{eh}/2m_e = 139$  K (a) and at density  $2m_e T/2\pi = 2.2 \times 10^{12}$  cm $^{-2}$  (b), and is hardly noticeable. The efficiency is high and nearly constant across the different regimes, so the optimal regime is at the maximum of the ET rate, that is, around the hole degeneracy point that occurs at  $n_{eh} = 2m_h T/2\pi$ .

## V. ENERGY TRANSFER INTO DISCRETE QD STATES

Throughout the paper, we assumed that the QD density of states was constant on the energy scale corresponding to variations of the transition matrix element of the free QW excitons. Experimentally, this situation occurs if the band gap of the QDs is much smaller than the band gap of the QW, so that the final states participating in the Förster transfers are in the quasicontinuum of high-energy QD excitations. If the band gaps of the QDs and the QW are close to each other, then the transfer excites discrete low-energy QD excitons. For the case of dispersionless localized QW excitons this will only change numerical prefactors in the Förster transition rate. However, as we show below, in the case of free QW excitons or free carriers, we obtain a different behavior for the ET rate if the width of the QD transition is small compared to the scale, on which significant variations of the ET transition matrix element occur.

If the width of the QD exciton is smaller than  $1/2MR^2$ , we can approximate the exciton line by a delta function and obtain

$$\frac{1}{\tau_{F,\delta}(K)} \sim \left(\frac{e^2}{\epsilon}\right)^2 |d_D|^2 |d_W|^2 \frac{n_D}{a_B^2} K^2 e^{-2KR} \delta\left(\frac{K^2}{2M} - E_D\right), \quad (31)$$

where  $E_D$  is the energy of the QD exciton measured with respect to the bottom of the QW exciton band. The use of the Fermi Golden Rule is justified if the rate  $1/\tau_{F,\delta}(K)$  is smaller than the dephasing rate of the QD exciton (determined by its linewidth). The latter condition is usually satisfied in real QW/nanocrystal QD systems, because the ET rate is in the submicroelectron-volt range, while the widths of nanocrystal transitions even at low temperatures are in the submillielectron-volt-to-millielectron-volt range.<sup>20,21</sup>

The thermal averaging will lead to the replacement

$$\frac{N_D}{R^2}(E_G)f(2MTR^2) \rightarrow \frac{ME_D}{T} e^{-2R\sqrt{2ME_D} - \frac{E_D}{T}}. \quad (32)$$

We see that at large  $T$ , the dependence of the rate is still  $\propto 1/T$  as in the case of high-energy quasicontinuous QD excitations. However, the QW-QD distance dependence changes completely. While the ET rates calculated in the Secs. III and IV follow approximately the  $R^{-4}$  dependence [ $f(2MTR^2) \propto R^{-2}$  for large  $R$ ], the ET rates in the case of transfer into discrete QD states depend exponentially on the QW-QD separation. The rate of the exponential distance decay can be controlled by the QW-QD energy offset  $E_D$ . In the resonant case,  $E_D$  is nonzero but is determined by the inhomogeneous broadening of the QD transition energy. Typical QDs are synthesized with a narrow size dispersion of approximately 7%, which translates into an energy variation  $\Delta E$  of  $\sim 50$  meV around a center energy of 2.2 eV. Assuming that in the ‘‘quasiresonant’’ case  $E_D = \Delta E$ , we find that the ET rate decreases on a very short length scale of  $\sim 5$  Å.

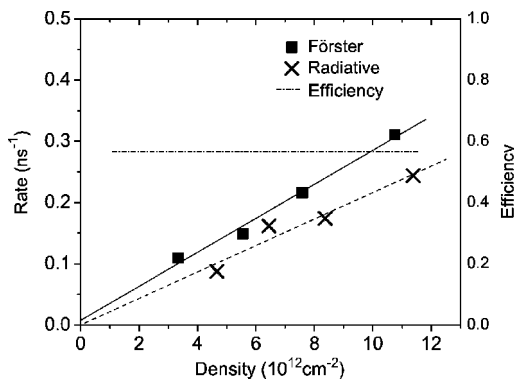


FIG. 4. Experimental results: Förster (squares) and radiative recombination rates (crosses) as a function of excited carrier density (the solid and dashed lines are guides to the eye). The dash-dotted line is the ET efficiency ( $\eta=57\%$ ).

## VI. EXPERIMENT: ENERGY TRANSFER BETWEEN AN InGaN QW AND CdSe QDs

In this section, we compare our theoretical calculations with results of the measurements that we perform for the hybrid structure schematically shown in Fig. 1. In our experimental work we use optical excitation (see below), therefore, the QW in our device does not have metal contacts. The structure consists of a close-packed monolayer of CdSe/ZnS core/shell nanocrystal QDs deposited by the Langmuir-Blodgett technique on an InGaN/GaN heterostructure. The 30 Å wide InGaN quantum well is capped with a thin, 30 Å thickness GaN top barrier layer. We excite the hybrid QW/QD structure at 266 nm with 100 fs laser pulses from a frequency-tripled, amplified Ti:sapphire laser and measure the dynamics of the QW emission at 400 nm using a time-correlated single photon counting system.<sup>14</sup> First, we measure the PL dynamics from an isolated QW without QDs in its proximity. From the quadratic carrier density dependence of the PL amplitude at zero time delay we conclude that the QW excitation can be described by nondegenerate free carriers. Despite the large “nominal” exciton binding energy (675 K), charge carriers in InGaN QWs do not form excitons at room temperature because of strong piezoelectric fields.<sup>22</sup>

For the free carrier case we would expect a PL decay rate that depends linearly on the carrier density [Eq. (26)]. However, we find a nonvanishing decay rate of  $1 \text{ ns}^{-1}$  at low carrier densities that we attribute to nonradiative recombination as a result of carrier trapping at defects (typically observed for InGaN QWs at room temperature). After subtracting this nonradiative contribution from the decay dynamics, we obtain the radiative recombination rate (Fig. 4) that shows the expected linear carrier density dependence. The experimental and calculated radiative rates agree within a factor of 2. Next, we compare the QW PL decay dynamics of

the isolated QW (decay rate  $1/\tau_{w/o \text{ QDs}}$ ) with the dynamics measured for the hybrid QW/QD structure (decay rate  $1/\tau_{with \text{ QDs}}$ ). We find an accelerated PL decay in the hybrid structure as a result of ET from the QW to the QDs. The ET rate ( $1/\tau_F = 1/\tau_{w/o \text{ QDs}} - 1/\tau_{with \text{ QDs}}$ ) is plotted in Fig. 4. Both the linear carrier density dependence and the absolute values of the measured ET rate are in agreement with Eq. (22) and Fig. 3, respectively. The ET efficiency of 57% (see Ref. 23) that we calculated from the measured ET and radiative recombination rate is close to the theoretical value of 80%.

## VII. SUMMARY AND CONCLUSIONS

We have studied the rate of nonradiative Förster energy transfer between a quantum well and a proximal layer of nanocrystal QDs. We considered both the low-density/low-temperature regime, in which the excitations are bound excitons either free or localized [Eqs. (15) and (20)] and the high-density/high-temperature regime in which the electrons and holes form a plasma of free charge carriers, in the non-degenerate [Eqs. (22) and (26)], degenerate [Eqs. (24) and (27)], or intermediate degenerate/nondegenerate [Eq. (28)] regimes. For the numerical estimations, we used physical parameters from the experiments reported in Ref. 14. For the case of QW excitons, we find that the energy transfer into the QDs is optimal if the contribution from the localized excitons is negligible and if the temperature is on the order of the exciton kinetic energy with momentum equal to the inverse of the distance between the quantum well and the layer of the quantum dots. For the case of free carriers in the quantum well, we find that the energy transfer is optimal around the hole degeneracy temperature. In addition, we considered ET to discrete QD states. For this configuration, we found that the ET rates decay exponentially with increasing QW-QD separation. The characteristic distance turned out to be very small, on the order of a few angstroms. Finally, we validated the theoretical model by comparing our calculations with experimental results obtained for a hybrid InGaN QW/CdSe QD device. We measured ET rates, radiative recombination rates, and ET efficiencies and found a good agreement with our theoretical predictions for the case of free carriers in the QW. Independently we confirm that under our experimental conditions QW excitations are indeed present in the form of free carriers. In conclusion, our results indicate that with a careful design of the system (geometrical and electronic parameters), the Förster transfer can be used as an efficient “noncontact” pumping mechanism of nanocrystal QD-based light emitting devices.

## ACKNOWLEDGMENTS

This project was supported by Los Alamos LDRD Funds and the Chemical Sciences, Biosciences, and Geosciences Division of the Office of Basic Energy Sciences, Office of Science, U.S. Department of Energy.

\*Present address: Theory of Condensed Matter Group, Cavendish Laboratory, Cambridge, CB3 0HE, United Kingdom.

- <sup>1</sup>A. P. Alivisatos, *Science* **271**, 933 (1996).
- <sup>2</sup>C. B. Murray, D. J. Norris, and M. G. Bawendi, *J. Am. Chem. Soc.* **115**, 8706 (1993).
- <sup>3</sup>M. A. Hines and P. Guyot-Sionnest, *J. Phys. Chem.* **100**, 468 (1996).
- <sup>4</sup>B. O. Dabbousi, J. Rodriguez-Viejo, F. V. Mikulec, J. R. Heine, H. Mattoussi, R. Ober, K. F. Jensen, and M. G. Bawendi, *J. Phys. Chem. B* **101**, 9463 (1997).
- <sup>5</sup>L. Qu and X. Peng, *J. Am. Chem. Soc.* **124**, 2049 (2002).
- <sup>6</sup>*Semiconductor and Metal Nanocrystals: Synthesis and Electronic and Optical Properties*, edited by V. I. Klimov (Marcel Dekker, New York, 2003).
- <sup>7</sup>C. B. Murray, C. B. Kagan, and M. G. Bawendi, *Science* **270**, 1335 (1995).
- <sup>8</sup>M. Achermann, M. A. Petruska, S. A. Crooker, and V. I. Klimov, *J. Phys. Chem. B* **107**, 13782 (2003).
- <sup>9</sup>S. A. Crooker, J. A. Hollingsworth, S. Tretiak, and V. I. Klimov, *Phys. Rev. Lett.* **89**, 186802 (2002).
- <sup>10</sup>V. Colvin, M. Schlamp, and A. Alivisatos, *Nature (London)* **370**, 354 (1994).
- <sup>11</sup>B. O. Dabbousi, M. G. Bawendi, O. Onitsuka, and M. F. Rubner, *Appl. Phys. Lett.* **66**, 1316 (1995).
- <sup>12</sup>N. Tessler, V. Medvedev, M. Kazes, S. Kan, and U. Banin, *Science* **295**, 1506 (2002).
- <sup>13</sup>S. Coe, Wing-Keung Woo, M. Bawendi, and V. Bulovic, *Nature (London)* **420**, 800 (2002).
- <sup>14</sup>M. Achermann, M. A. Petruska, Š. Kos, D. L. Smith, D. D. Koleske, and V. I. Klimov, *Nature (London)* **429**, 642 (2004).
- <sup>15</sup>V. M. Agranovich, D. M. Basko, G. C. La Rocca, and F. Bassani, *J. Phys.: Condens. Matter* **10**, 9369 (1998).
- <sup>16</sup>D. Basko, G. C. La Rocca, F. Bassani, and V. M. Agranovich, *Eur. Phys. J. B* **8**, 353 (1999).
- <sup>17</sup>For a review of optical processes in quantum wells, see, e.g., E. Runge, *Solid State Phys.* **57**, 149 (2002).
- <sup>18</sup>P. Lawaetz, *Phys. Rev. B* **4**, 3460 (1971).
- <sup>19</sup>We assume charge neutrality, that is  $n_e = n_h \equiv n_{eh}$ .
- <sup>20</sup>S. A. Empedocles, D. J. Norris, and M. G. Bawendi, *Phys. Rev. Lett.* **77**, 3873 (1996).
- <sup>21</sup>H. Htoon, P. J. Cox, and V. I. Klimov, *Phys. Rev. Lett.* **93**, 187402 (2004).
- <sup>22</sup>O. Ambacher, J. Majewski, C. Miskys, A. Link, M. Hermann, M. Eickhoff, M. Stutzmann, F. Bernardini, V. Fiorentini, V. Tilak, B. Schaff, and L. F. Eastman, *J. Phys.: Condens. Matter* **14**, 3399 (2002).
- <sup>23</sup>To compare measured and calculated ET efficiencies we only consider radiative recombination and disregard nonradiative decay processes.